frontiers | Frontiers in Earth Science

TYPE Original Research
PUBLISHED 20 May 2024
DOI 10.3389/feart.2024.1411126

OPEN ACCESS

EDITED BY
Yongqiang Chen,
Commonwealth Scientific and Industrial Research Organisation (CSIRO), Australia

REVIEWED BY
Zhiyang Li,
Texas A&M International University, United States
Feng Wu,
Southwest Petroleum University, China
Tao Nian,
Xi'an Shiyou University, China

*CORRESPONDENCE
Zhiwei Wu,
2022710367@yangtzeu.edu.cn

RECEIVED 02 April 2024
ACCEPTED 02 May 2024
PUBLISHED 20 May 2024

CITATION
Yuan R, Wu Z, Xin Y, Zhang H, Wu S and Yang S (2024), Utilizing logs to identify complex lithology of tight marl reservoir in the Leikoupo Formation 3^2 Submember ($T_2l_3^2$) of the Sichuan Basin, China. *Front. Earth Sci.* 12:1411126. doi: 10.3389/feart.2024.1411126

Utilizing logs to identify complex lithology of tight marl reservoir in the Leikoupo Formation 3^2 Submember ($T_2l_3^2$) of the Sichuan Basin, China

Rui Yuan[1], Zhiwei Wu[1]*, Yongguang Xin[2], Hao Zhang[2], Saijun Wu[3] and Siyue Yang[1]

[1]School of Geophysics and Petroleum Resources, Yangtze University, Wuhan, Hubei, China, [2]Sichuan Basin Research Center, PetroChina Research Institute of Petroleum Exploration and Development, Chengdu, Sichuan, China, [3]PetroChina Research Institute of Petroleum Exploration and Development, Beijing, China

Recent exploration has revealed that the Middle Triassic Leikoupo Formation 3^2 Submember ($T_2l_3^2$) in the Sichuan Basin contains unconventional marl reservoirs with significant natural gas potential. Due to limited cores, old wells, and conventional logs, however, the lithological understanding of $T_2l_3^2$ is incomplete and relies solely on inaccurate mud logs. This lack of lithological foundation challenges geology and petroleum research. To identify complex lithology, this paper presents a double-hierarchical workflow to identify seven types of lithology using logs. The first order distinguishes salt, anhydrite, and marl, while the second order further subdivides marl into anhydrite marl, argillaceous limestone, shaly limestone, and limy shale. Different rocks' logging response characteristics are summarized based on quantity-limited cores and micro-resistivity imaging logs. Lithological identification of 2D and 3D plots is established using sensitive GR, DEN, and RT. Corresponding identification standards are built in two hierarchies. According to these standards, the lithology of $T_2l_3^2$ is identified in a total of 119 wells. Finally, the lithological characteristics of vertical, horizontal, and plane are discussed in the research area. The research results may aid in comprehending the entire lithological characteristics of the complex marl reservoir in $T_2l_3^2$ of the Sichuan Basin. It would help the exploration potential of petroleum systems in turn.

KEYWORDS

logs, complex lithology, tight marl, Leikoupo Formation, Sichuan Basin

1 Introduction

The identification of lithology is the foundation of petroleum resource exploration and development. Drilling cores provide direct evidence of subsurface strata. However, they are costly and time-consuming. Mud logs offer initial information in drilling formation, but their lithological data is rough and inaccurate. These lithological results are unsuitable for detailed descriptions of oil and gas reservoirs. Various well logs record multiple physical properties of stratigraphy within high resolution, which are the widespread data in each

open hole. The identification of lithology using logs is the most effective and direct method for recognizing subsurface rocks of formation (Kumar et al., 2018; Ramos and Neves, 2019; Saporetti et al., 2019).

Carbonate is one kind of significant hydrocarbon reservoir with complex lithology, including limestone, dolomite, anhydrite, salt, and other rocks (Paul and Stephen, 2006; Ben et al., 2019). Carbonate reservoirs are essential natural gas producers in China (Chen et al., 2022). Dozens of carbonate gas fields have been built in the Sinian, Cambrian, and Permian of the Sichuan Basin of China (Ma et al., 2008; Tan et al., 2011; Wang L. et al., 2020; Liao et al., 2020; Tan et al., 2021). Specifically, the Middle Triassic Leikoupo Formation 3^2 Submember ($T_2l_3^2$) in the central Sichuan Basin has yielded 3×10^5 m^3 gas and 47.04 m^3 oil per day in oil tests of CT1 Well in 2020 (Wang et al., 2023). It is a breakthrough in the marl intervals of $T_2l_3^2$, which kicked off the hydrocarbon exploration in this formation (Shen et al., 2008; Zhou et al., 2010; Xin et al., 2013a; Xin et al., 2013b; Lü et al., 2013; Tian et al., 2018; Wang X. et al., 2020; Tian et al., 2020; Tian et al., 2021; Zhang et al., 2021; Xin et al., 2022). Marl is a type of complex carbonate that is often a mixture of mud and limestone (Balumi et al., 2022; Yin et al., 2023). Marl reservoir exhibits poor physical properties, with porosity ranging from 2% to 8% and permeabilities of $(0.001–1) \times 10^{-3}$ μm^2 in $T_2l_3^2$. Due to limited cores, imprecise mud logs, and old well data, obtaining accurate geological information would be difficult in the $T_2l_3^2$ formation. In this paper, a hierarchical lithological identification method from logs is formed to solve the lithological problem of tight marl reservoir in $T_2l_3^2$ effectively. Log response characteristics of different rocks are summarized on the quantity-limited cores and micro-resistivity imaging log. Corresponding 2D and 3D lithological plots are established. Finally, the lithological characteristics of $T_2l_3^2$ are discussed.

2 Geological setting

2.1 Tectonic and depositional background

Yangtze Para-platform is a significant platform for the Chinese mainland. The Sichuan Basin is in the northwestern Yangtze Para-platform as a secondary tectonic unit. For the early tectonic uplift in the Indo-China Movement, the Sichuan Basin was enclosed by palaeo-highs and palaeo-lands in the Yangtze Cratonic Block. In the Middle Triassic Leikoupo Stage, therefore, the Sichuan Basin was a part of the Yangtze Craton Basin. Sichuan Basin adjoined Yunnan-Tibet Palaeo-ocean in the west through Longmen Mountain Island-chain; adjoined Qinling Palaeo-ocean and Northern Qinling Palaeo-land in the north by Michang and Daba Mountain Uplift; and was surrounded by Kangdian Palaeo-land in the southwest and Jiangnan Palaeo-land in the east. In the Sichuan Basin, Chuanxi, Chuanzhong, and Chuandong Depressions, and Kaijing and Luzhou Uplifts (Figure 1A) (Tian et al., 2021). This palaeogeographic framework of the Sichuan Basin in the Leikoupo Stage results in the depositional environment of an evaporated-restricted platform. Mixed lagoon and flat were widely distributed in the $T_2l_3^2$ of the Sichuan Basin. In the central basin, depositional facies were mainly developed in marly and anhydrite lagoon and marly flat, which is the dominant research region of this paper (Figure 1B) (Tian et al., 2021).

2.2 Stratigraphic background

According to the stratigraphy in the Sichuan Basin, the Middle Triassic Leikoupo Formation is divided into five members, named Lei-1 (T_2l_1), Lei-2 (T_2l_2), Lei-3 (T_2l_3), Lei-4 (T_2l_4), and Lei-5

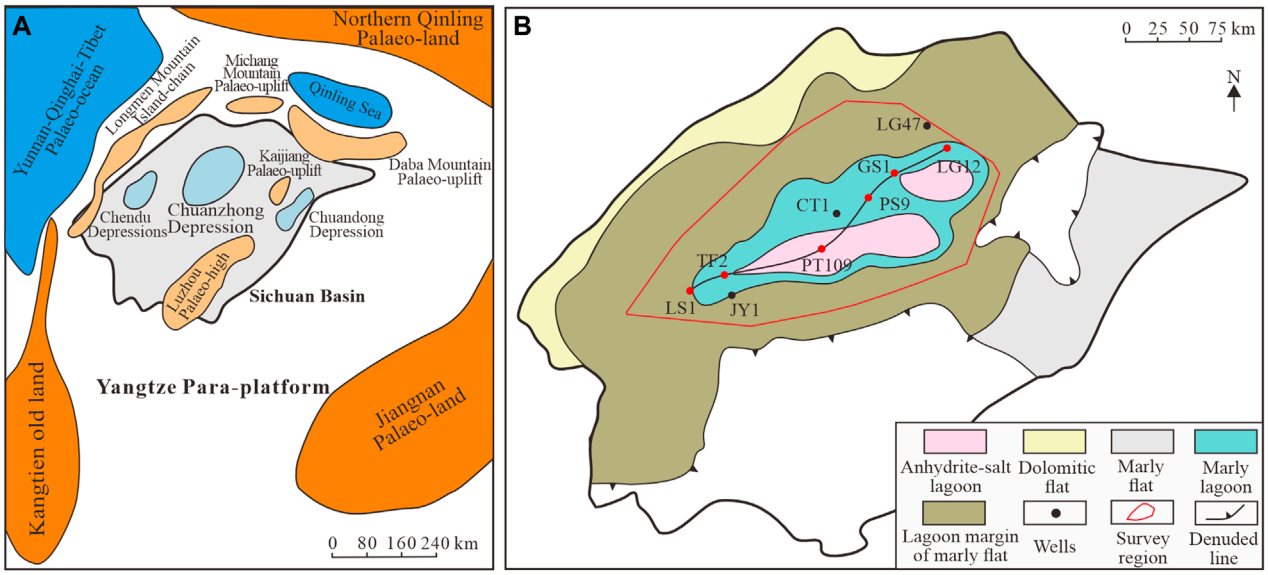

FIGURE 1
Tectonic of the Sichuan Basin and depositional background of $T_2l_3^2$. **(A)** Tectonic background of the Sichuan Basin (modified from Tian et al., 2021). **(B)** Depositional background of $T_2l_3^2$ in the Sichuan Basin (modified from Tian et al., 2021).

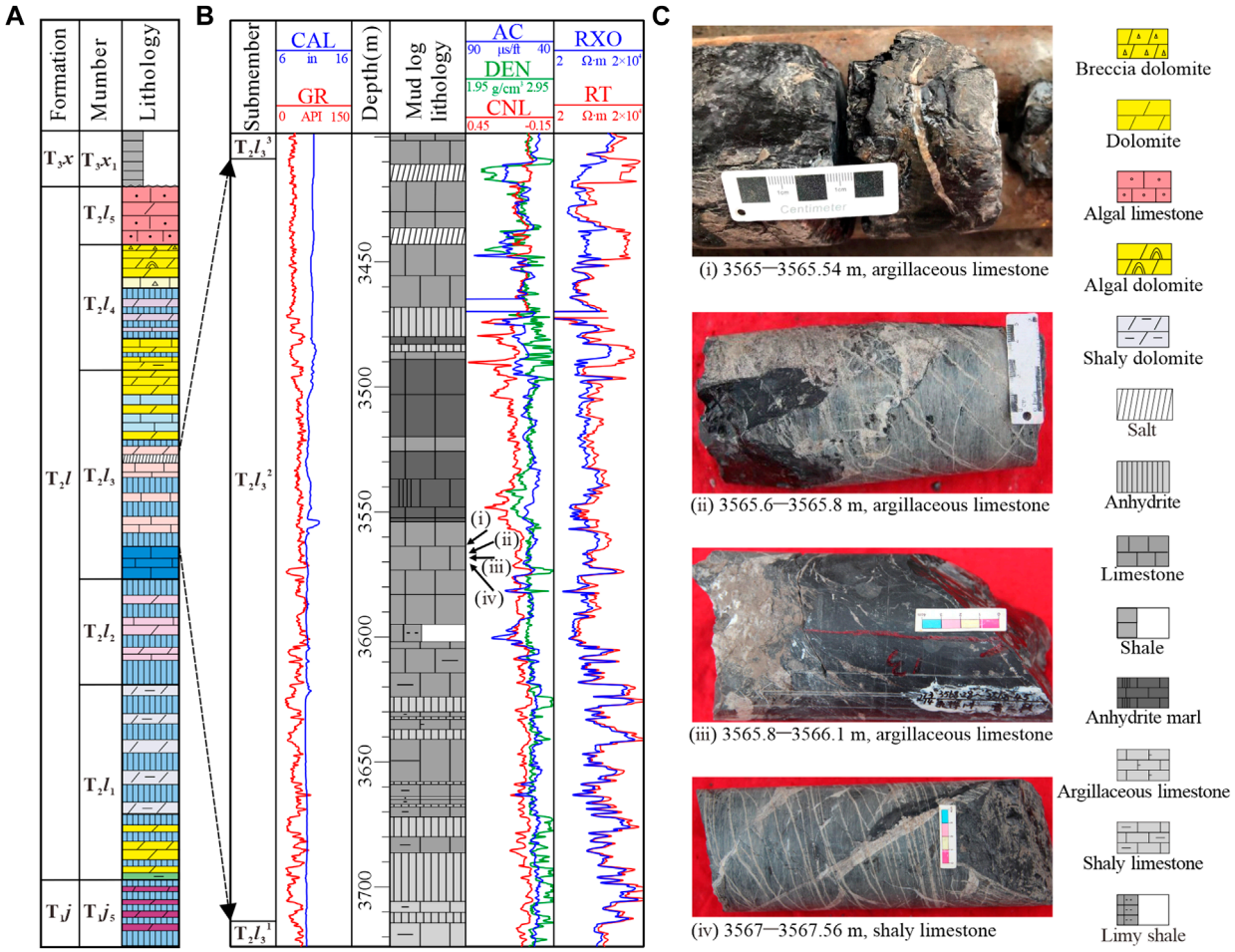

FIGURE 2
Stratigraphic characteristics of the $T_2l_3^2$ in the central Sichuan Basin. **(A)** Lithological characteristics of the Leikoupo Formation. **(B)** Generalized open-hole stratigraphic $T_2l_3^2$ of CT1 Well. Conventional logs: CAL-borehole diameter (in), GR-natural gamma ray (API), AC-acoustic time (μs/ft), DEN-compensated bulk density (g/cm^3), CNL-compensated neutron (decimal), RT-deep investigation resistivity (Ω·m), RXO-shallow investigation resistivity (Ω·m). **(C)** Core description and photos in CT1 Well.

(T_2l_5) upwards (Figure 2A). Within a thickness of 200 m, the Lei-3 Member is further subdivided into three submembers, termed 3^1 ($T_2l_3^1$), 3^2 ($T_2l_3^2$), and 3^3 ($T_2l_3^3$) upwards. $T_2l_3^2$ is approximately 100 m thick and is the main gas pay of the T_2l_3. Based on current geological understanding, $T_2l_3^2$ is composed of six dominant lithologies: salt, anhydrite, anhydrite marl, argillaceous limestone, shaly limestone, and limy shale (Figure 2B). Oilfield petrologists consider that hydrocarbon would be generated in the limy shale and enriched in the shaly limestone; the salt and anhydrite are cover rocks. Therefore, the whole $T_2l_3^2$ is considered as a "self-generation and self-storage" complex unconventional marl gas reservoir (Yang et al., 2022; Zhang et al., 2023).

3 Data and methods

3.1 Database

In the central Sichuan Basin, more than one hundred wells have been drilled in $T_2l_3^2$. Almost all wells have been run by conventional logs, including borehole diameter (CAL, in), natural gamma ray (GR, API), deep resistivity (RT, Ω·m), shallow resistivity (RXO, Ω·m), acoustic time (AC, μs/ft), compensated neutron (CNL, decimal) and bulk density (DEN, g/cm^3) (Figure 2B). 119 wells are involved in this paper. Although cuttings while drilling were recorded to understand the lithology of formation, this information is in large error. Therefore, coring has become an important criterion for lithological identification. For the long drilling time and high coring cost, just two coring runs (8.65 m) and one coring run (8.4 m) were operated in CT1 and JY1 Well respectively (Figure 2C). Meanwhile, micro-resistivity imaging logs were generated in JY1 Well. These ultrahigh-resolution images cover the shortage of cores and play an important role in describing lithology and fabric of formation finely (Zhou, 2008; Xu et al., 2009; Yan et al., 2011; Folkestad et al., 2012; Brekke et al., 2017; Luo et al., 2018; Zhang et al., 2018; Yuan et al., 2020).

3.2 Methods

The method of using well logs to identify lithology of complex unconventional marl reservoir in $T_2l_3^2$ of the Sichuan Basin requires

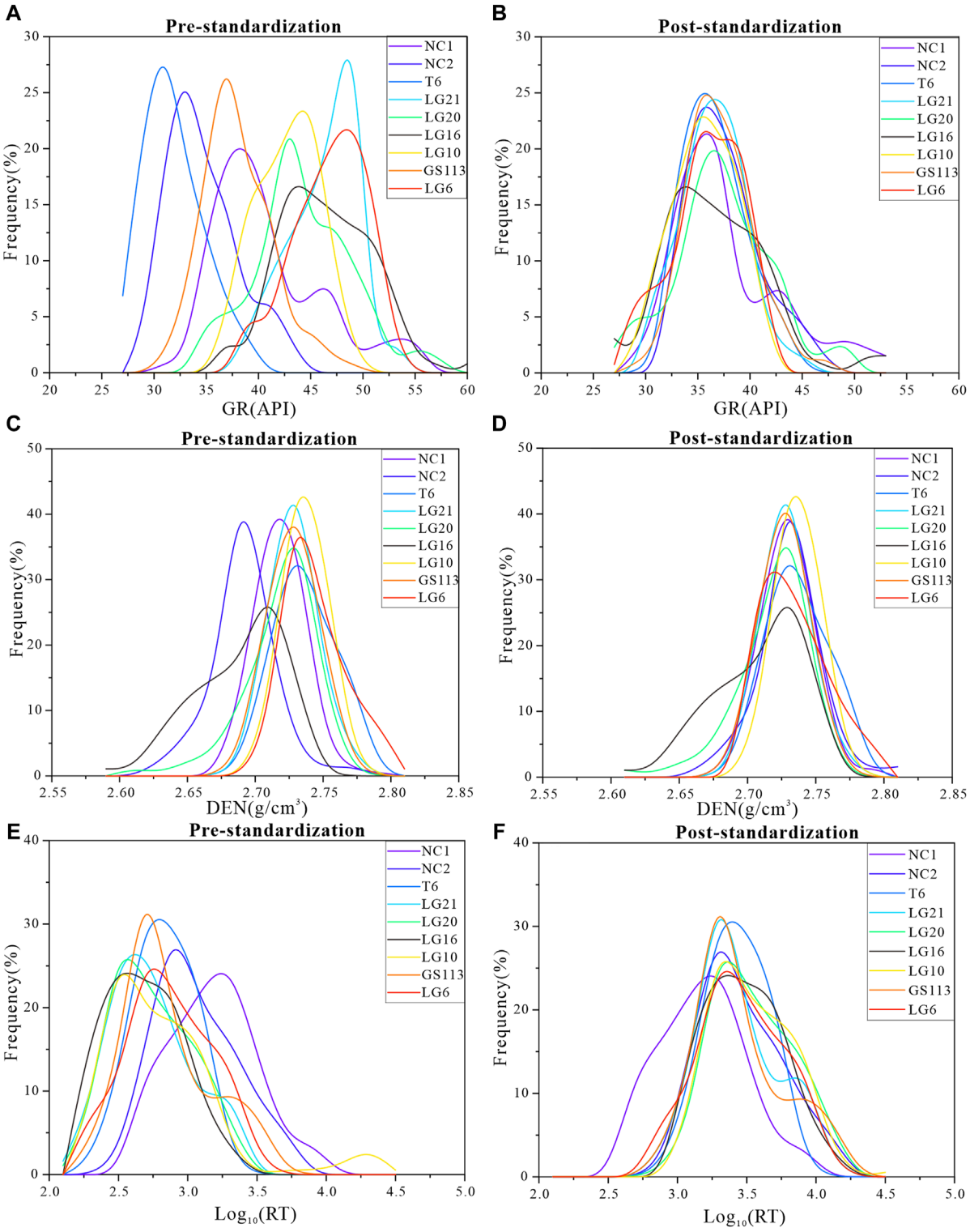

FIGURE 3
Standardization of logging curves in some wells. **(A)** Pre-standardization of GR. **(B)** Post-standardization of GR. **(C)** Pre-standardization of DEN. **(D)** Post-standardization of DEN. **(E)** Pre-standardization of RT. **(F)** Post-standardization of RT.

knowledge of primary carbonate and comprises five stages in this article. The first stage is the pre-processing of multiple data. All logging curves involved are standardized to eliminate systematic errors between logging tools (Figure 3). Depth of cores and borehole electrical images are corrected to the depth of logging curves in CT1 and JY1 Well. High-resolution 256-grayscale electrical conductivity

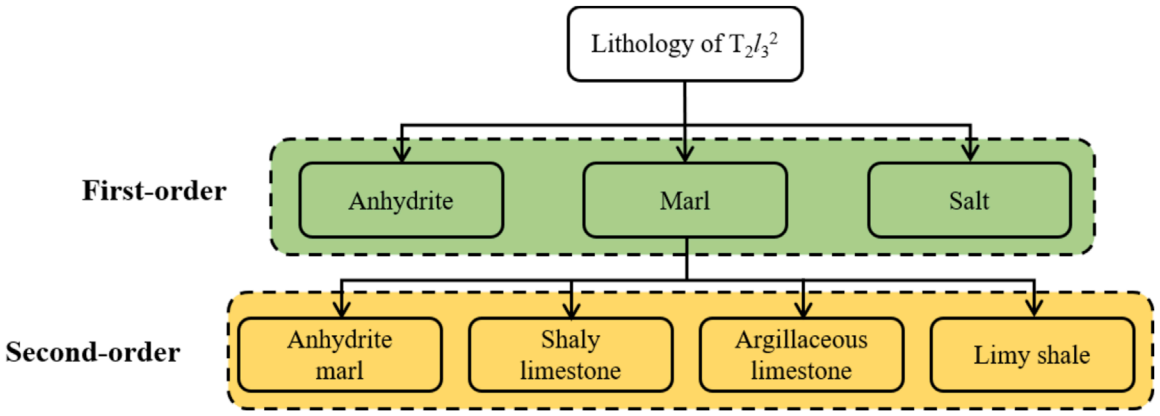

FIGURE 4
Hierarchical workflow of lithological identification in $T_2l_3^2$.

images are generated in JY1 Well. The second stage makes the applicable lithological identification hierarchical workflow. In the first-order, three categories of rocks are distinguished: salt, anhydrite, and marl. In the second-order, the marl is further subdivided into four types of lithology: anhydrite marl, argillaceous limestone, shaly limestone, and limy shale (Figure 4). The third stage summarizes the logging response characteristics of the above three categories and four types of lithologies. The lithological evidence comes from mud logs, cores, and micro-resistivity images. The fourth stage produces several 2D and 3D lithological plots hierarchically from logs. The fifth stage applies plots to identify lithology in boreholes and discusses the vertical, horizontal, and plane lithological characteristics of $T_2l_3^2$ in the Sichuan Basin.

4 Results

4.1 Logging response characteristics of different lithologies

Salt, anhydrite, and marl are the first-order lithologies in $T_2l_3^2$. Precipitated in evaporating sea and lake water, salt is a rock of pure chemical genesis. It consists mainly of halite, sylvine, gypsum, anhydrite, and so on minerals. Due to these chemical substances, salt is usually within the physical properties of high solubility, low radioactivity, low density, and non-conductivity (Wang et al., 2016; Zhang et al., 2022). It results in high CAL, low GR, low DEN, and high RT logging values in salt intervals (Shen et al., 2015; Xu et al., 2023). Similarly, with salt in a depositional environment, anhydrite is generated in highly concentrated water. In logging, anhydrite rocks have low GR, high DEN, and high RT normally (Carrasquilla and Caetano, 2021; Meng et al., 2022). Marl is a kind of transitional rock between carbonate and shale rock. Different from salt and gypsum, marl is characterized by medium-high GR, medium-low DEN, and medium-low RT in logging responses (Figure 5A) (Afsar et al., 2014; Cherif et al., 2021).

In second-order lithologies, anhydrite marl, argillaceous limestone, shaly limestone, and limy shale are finer lithologies in marl. Anhydrite marl is a type of mixture of anhydrite and marl. Marl is the primary material and anhydrite is the secondary mineral. The logging responses of anhydrite marl are between anhydrite and marl. In the micro-resistivity imaging logs, the anhydrite marl is blurry and massive. Argillaceous limestone, shaly limestone, and limy shale are mixed with calcareous and clay minerals. The content of clay minerals increases and that of calcareous minerals gradually decreases in these three lithologies. Theoretically, limestone has low radioactivity and low electrical conductivity. In contrast, clay is high in both of these characteristics. Therefore, these three fine lithologies would be carefully distinguished during logs. Limy shale has the highest GR and lowest RT; argillaceous limestone has the lowest GR and highest RT; logging responses of shaly limestone are intermediate between the above two lithologies. In the micro-resistivity imaging logs, argillaceous limestone, shaly limestone, and limy shale are alternated by horizontal dark and light stripes. Centimeter-thickness dark stripes indicate limy shale, while light bands indicate argillaceous limestone. Extreme thin dark and light stripes interbedding intervals imply shalylimestone (Figure 5B).

4.2 Lithological identification plots

Based on the logging response characteristics of different order lithologies, 2D and 3D lithological plots are produced, involving sensitive GR, DEN, and RT. Four plots are effective in distinguishing the first-order lithologies of salt, anhydrite, and marl. In the GR-DEN plot, salt is in the low GR and low DEN zone; anhydrite is in the low GR and high DEN zone (Figure 6A). In the RT-GR plot, marl is in the medium-high GR and low RT zone; salt and anhydrite are in low GR and high RT zone (Figure 6B). In the RT-DEN plot, marl is in medium DEN and low RT zone; salt is in low DEN and high RT zone; anhydrite is in high DEN and high RT zone (Figure 6C). These three lithologies are easily distinguished in the 3D GR-DEN-RT plot (Figure 6D). The corresponding identification standard would be: salt GR<35 API, DEN<2.5 g/cm^3, RT>3,000 Ω·m; anhydrite GR<35 API, DEN>2.7 g/cm^3, RT>800 Ω·m; marl GR>30 API, RT<2000 Ω·m, DEN 2.5–2.8 g/cm^3.

The GR-RT plate is also used to distinguish the second-order lithologies of anhydrite marl, argillaceous limestone, shaly

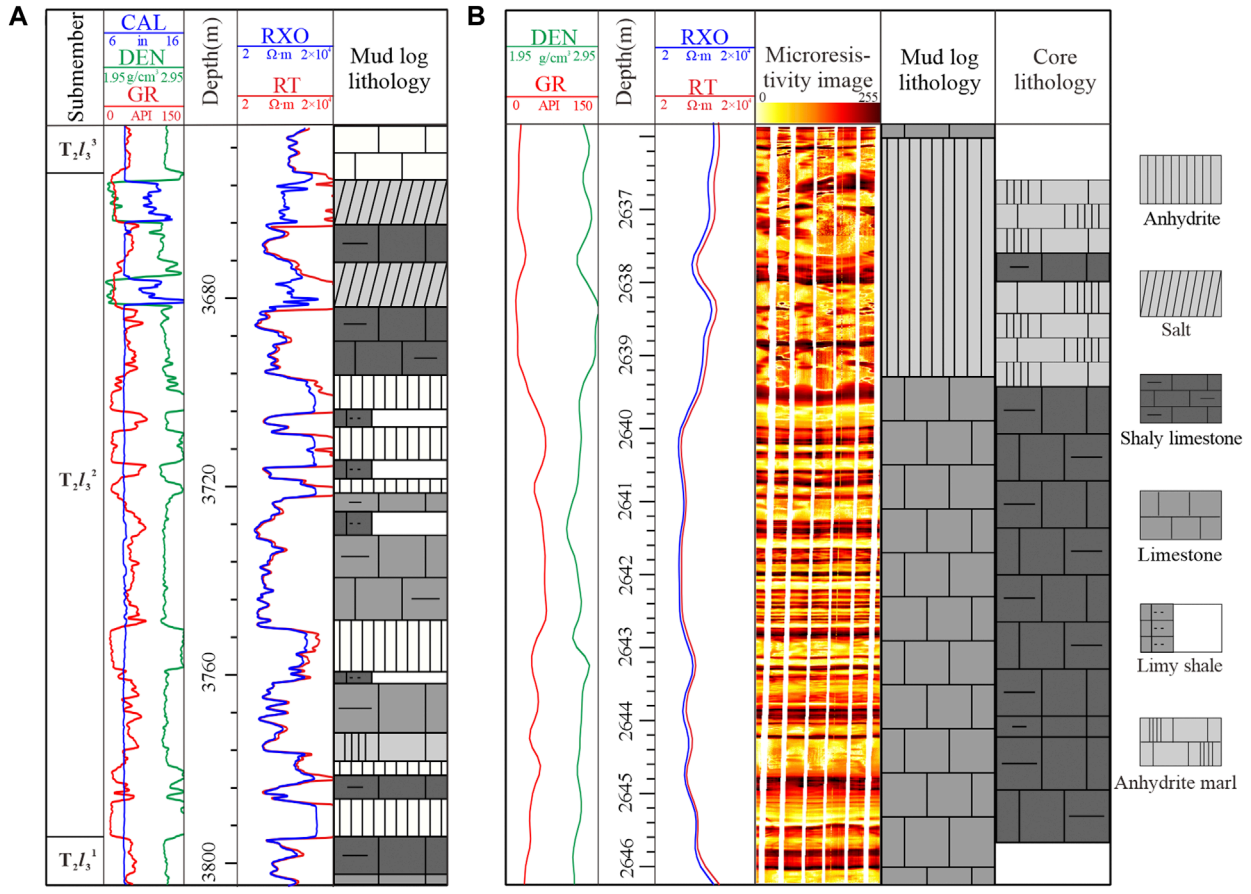

FIGURE 5
Logging response characteristics of different lithologies. **(A)** Logging response characteristics of first-order lithologies in GS1 Well. **(B)** Logging response characteristics of second-order lithologies in JY1 Well.

limestone, and limy shale in marl. Anhydrite marl is in the lowest GR and highest RT zone; limy shale is in the highest GR and lowest RT zone; argillaceous limestone is in low-medium GR and medium-high RT zone; shaly limestone is in medium GR and medium RT zone (Figure 7). The corresponding identification standard would be: anhydrite marl GR<35 API, RT 800–2000 Ω·m; argillaceous limestone GR 30–50 API, RT 200–2000 Ω·m; shaly limestone GR 40–60 API, RT 30–300 Ω·m; limy shale GR>45 API, RT<80 Ω·m. Finally, the logging lithological identification criteria for the $T_2l_3^2$ complex marl reservoir in the central Sichuan Basin are summarized in Table 1.

4.3 Compare identification results with cores

To check the availability of the lithological identification standard, identifying results are compared with core lithology in CT1 Well. In the coring interval, 3,560–3,568.65 m, upper lithology is argillaceous limestone and lower lithology is shaly limestone in coring description. In the lithological identification result, the interval of 3,561.8–3,562.54 m is in higher GR than up and down, and lithology is recognized as shaly limestone Figure 8. Coincidence rate between coring identifying and lithology is about 91%. Using the proposed method, centimeter-scale lithology would be acquired. In addition, the marl reservoir in $T_2l_3^2$ is very tight, within 2%–8% porosity. Water is hard to store in this tight marl reservoir. Gas and oil are usually in low saturation. Therefore, the logging responses are principally rooted in the rock framework. Different amount of pore fluids affects the GR, DEN, and RT finitely.

5 Discussion

5.1 Lithological characteristics in single well

Based on the above lithological identification standard for complex marl reservoir in $T_2l_3^2$, lithology is identified in a total of 119 wells. In the vertical formation, the lithological characteristics of $T_2l_3^2$ are obvious. Taking LG47 Well as an example, the lithological identification result is shown in Figure 9. The thickness of $T_2l_3^2$ is 213 m. In the mud log lithology, both anhydrite and marl are large sets of thick layers and no salt rock. In the lithological identification result, two salt layers, about 12 m thick, cover the upper formation. They are the significant cap rocks. Four main

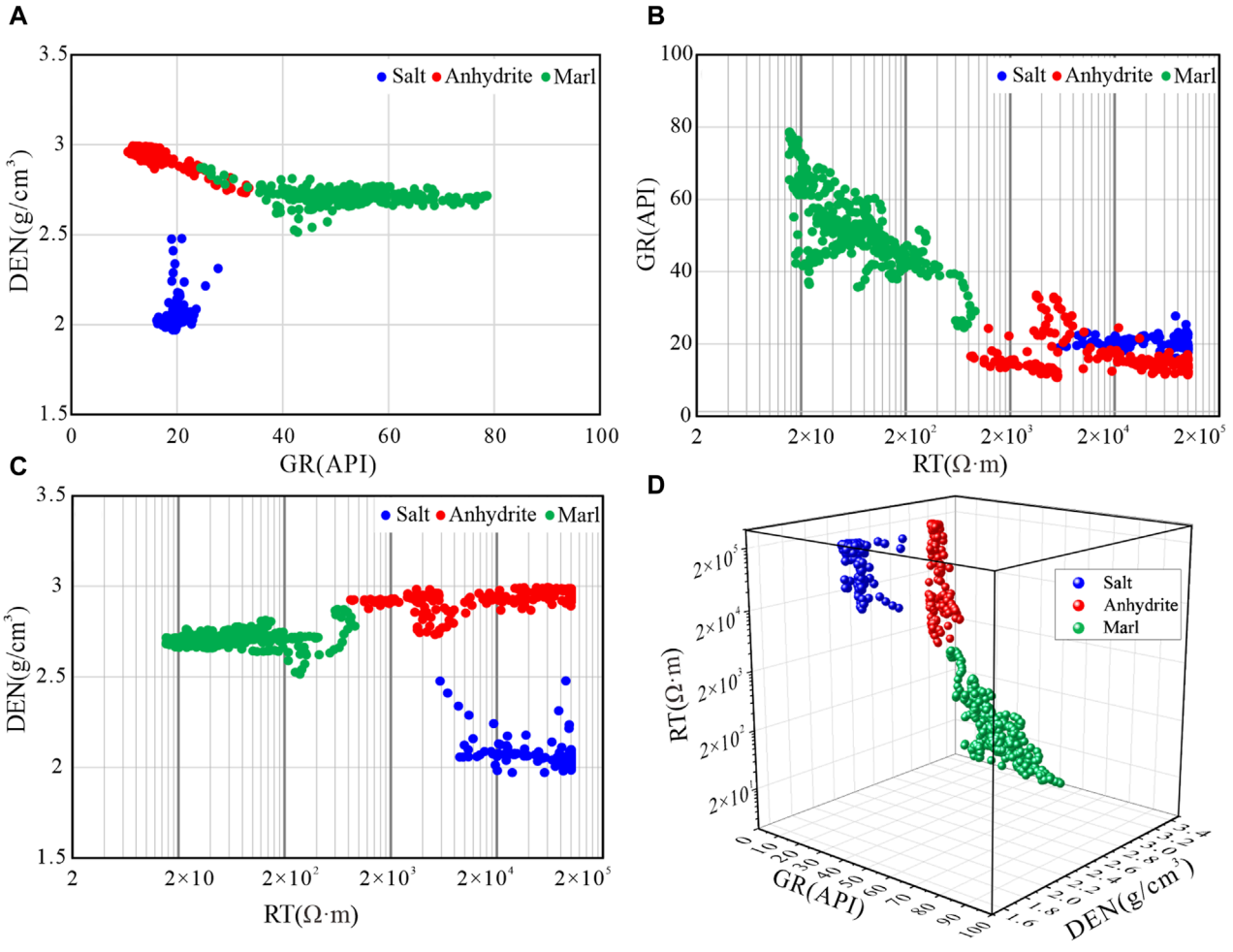

FIGURE 6
Lithological identification plots for the first-order lithologies of salt, anhydrite, and marl. Lithology and logging data derived from coring intervals of CT1 and JY1 Well. **(A)** 2D GR-DEN plot. **(B)** 2D RT-GR plot; **(C)** 2D RT-DEN plot; **(D)** 3D GR-DEN-RT plot.

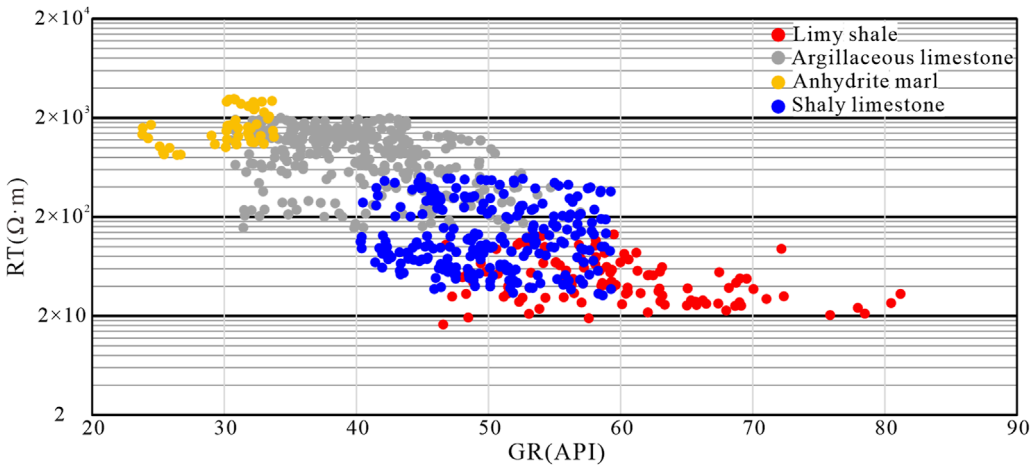

FIGURE 7
Lithological identification GR-RT plot for the second-order lithologies of anhydrite marl, argillaceous limestone, shaly limestone, and limy shale in marl. Lithology and logging data derived from coring intervals of JY1 Well.

10.3389/feart.2024.1411126

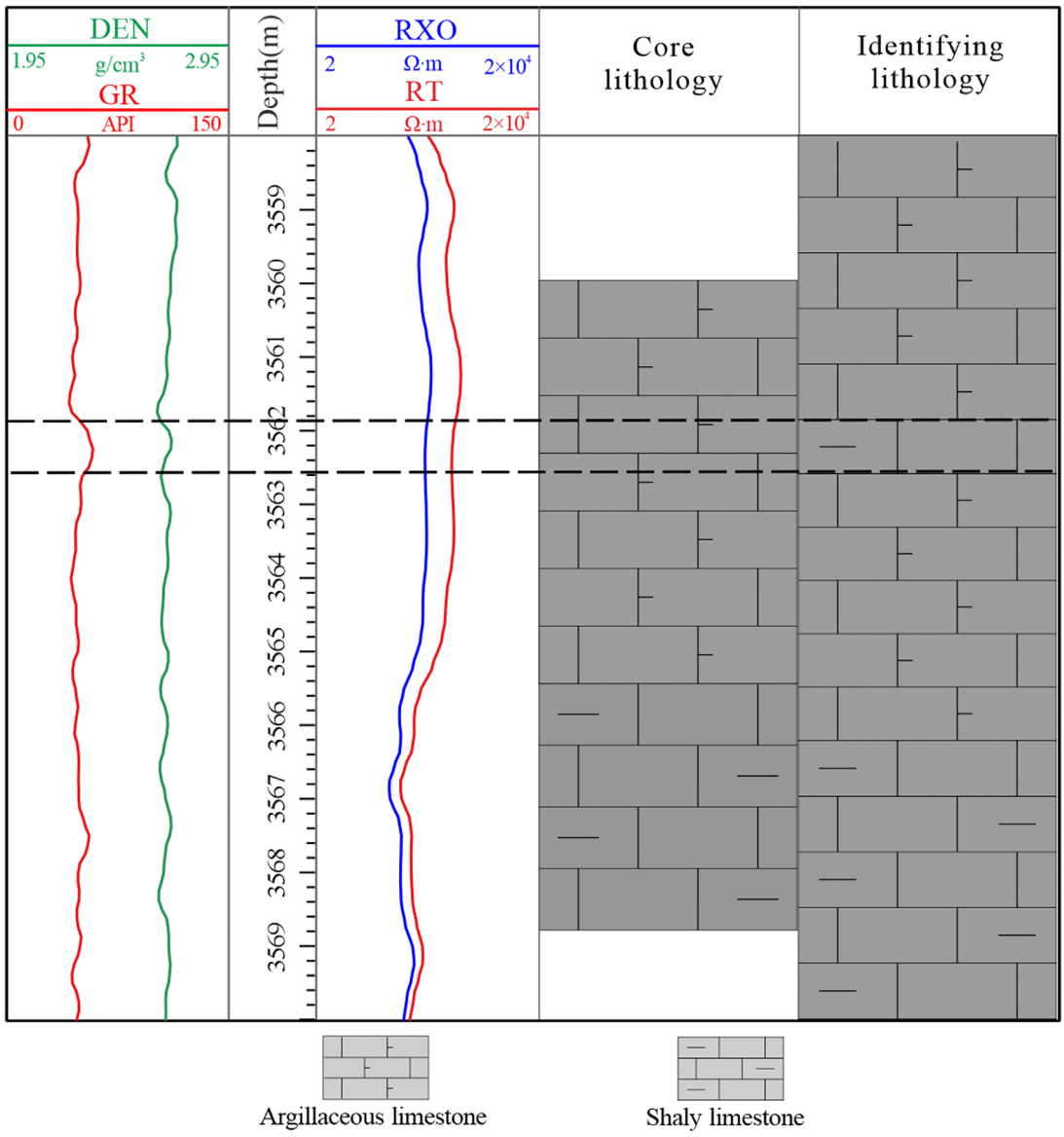

FIGURE 8
Compare identification results with cores in CT1 Well.

TABLE 1 Lithological identification standard of logs for complex marl reservoir of the $T_2l_3^2$ in the central Sichuan Basin.

Lithology		Logs		
First-order	Second-order	GR (API)	RT (Ω·m)	DEN (g/cm³)
Salt	—	<35	>3,000	<2.5
Anhydrite	—	<35	>800	>2.7
Marl	Anhydrite marl	<35	800–2000	2.5–2.8
	Argillaceous limestone	30–50	200–2000	
	Shaly limestone	40–60	30–300	
	Limy shale	>45	<80	

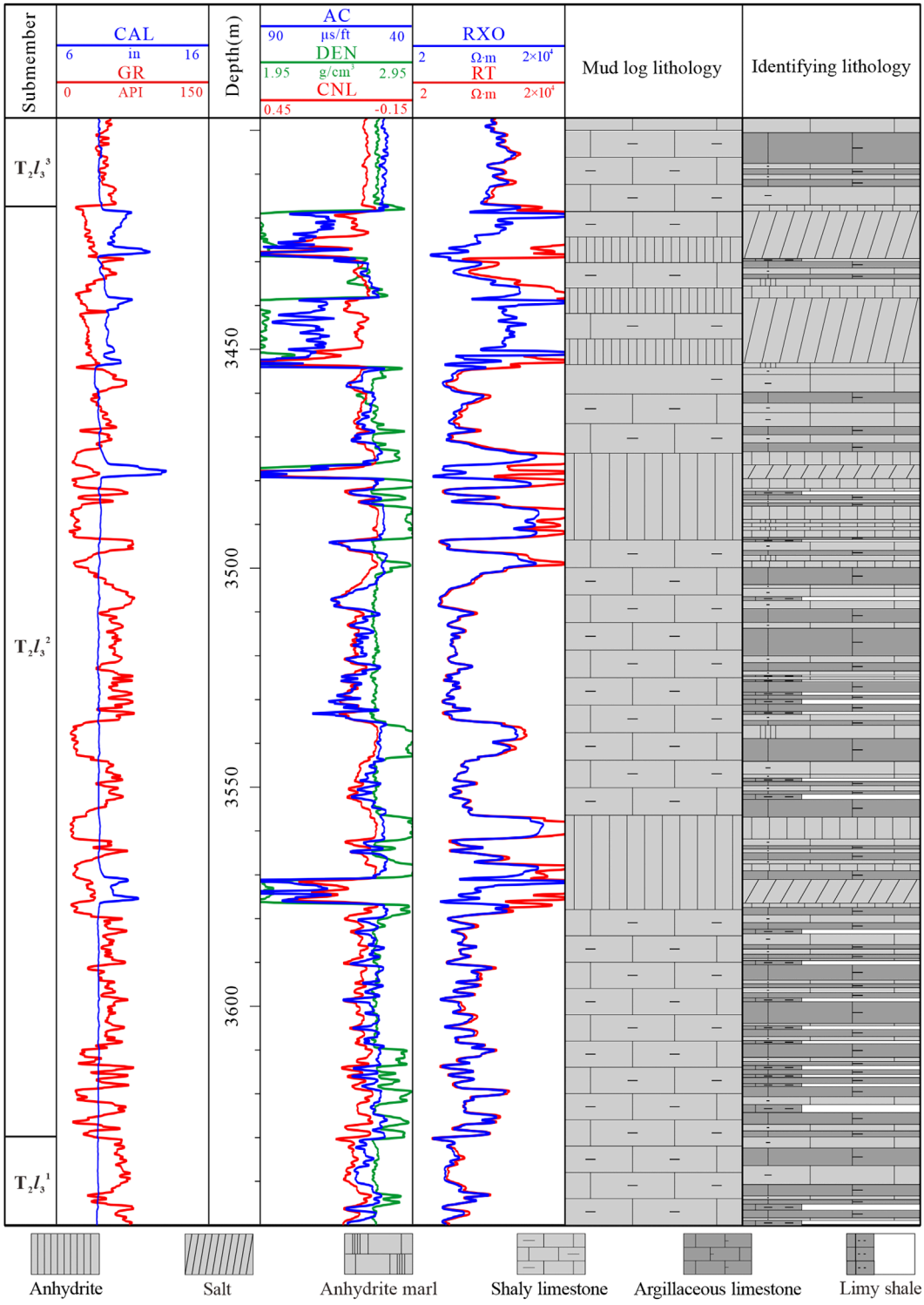

FIGURE 9
Lithological identification results of LG47 Well.

anhydrite layers, about 8 m thick, are developed in the middle formation. They are the interlayers between the marl reservoirs. Marl layers are thin and alternating. The number of layers, minimum thickness, average thickness, and maximum thickness of anhydrite marl is 8, 0.77 m, 1.58 m, and 3.23 m respectively. The number of layers, minimum thickness, average thickness, and maximum thickness of argillaceous limestone is 31, 0.5 m, 1.9 m, and 6.33 m respectively. The number of layers, minimum

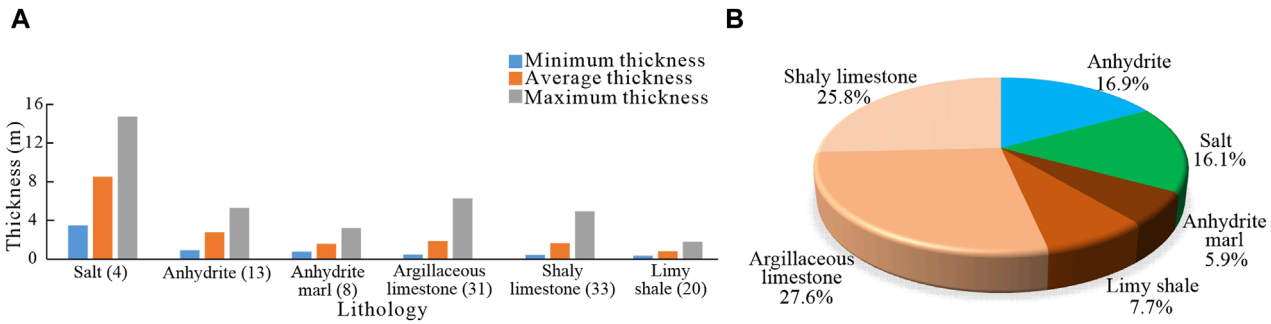

FIGURE 10
Quantitative thickness statistics of different lithologies. **(A)** Layer number, single layer minimum thickness, average thickness, and maximum thickness of different lithologies. Numbers in the brackets are layer numbers. **(B)** Total thickness percentage of different lithologies.

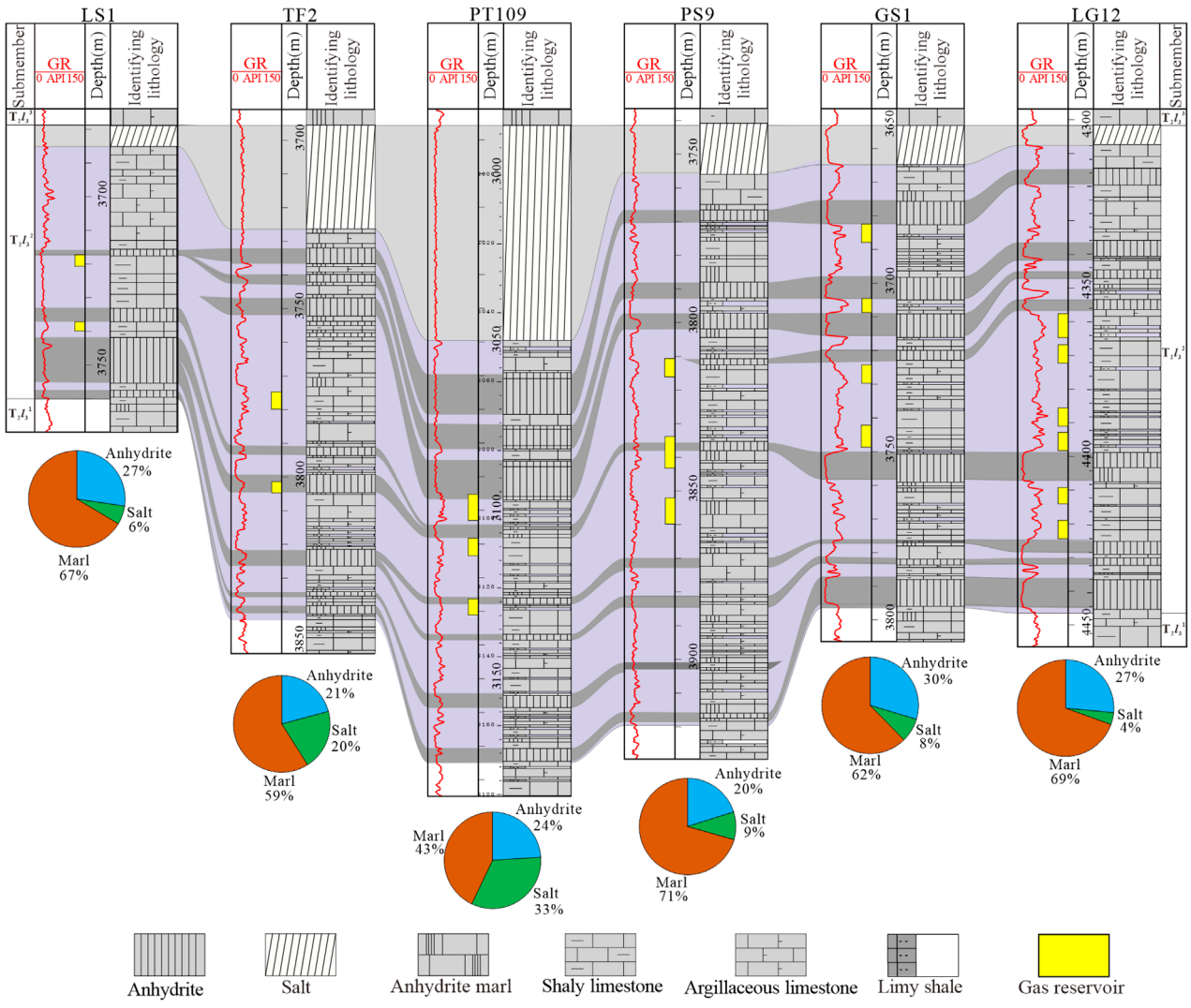

FIGURE 11
Lithological characteristics in the horizontal formation of $T_2l_3^2$. The location of the wells is marked in Figure 1B.

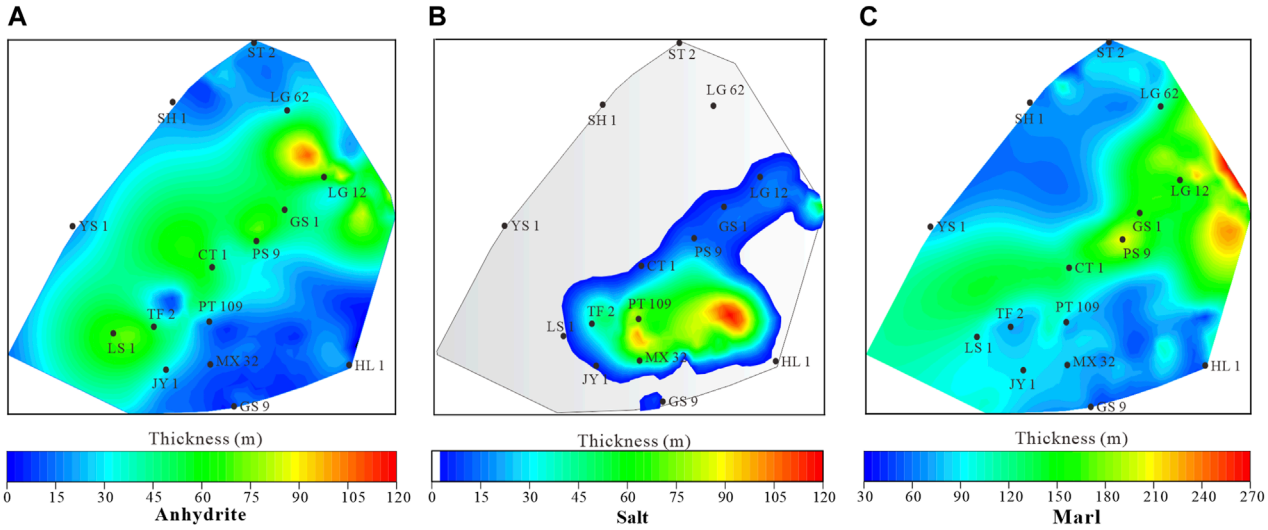

FIGURE 12
First-order lithological thickness plane spread of $T_2l_3^2$. **(A)** Thickness plane spread of anhydrite. **(B)** Thickness plane spread of salt. **(C)** Thickness plane spread of marl.

thickness, average thickness, and maximum thickness of shaly limestone is 33, 0.45 m, 1.67 m, and 4.98 m respectively. The number of layers, minimum thickness, average thickness, and maximum thickness of limy shale are 20, 0.35 m, 0.82 m, and 1.8 m respectively (Figure 10A).

In the entire $T_2l_3^2$ formation, the percentage of salt thickness is 16.1%; the percentage of anhydrite thickness is 16.9%; the percentage of anhydrite marl thickness is 5.9%; the percentage of argillaceous limestone thickness is 27.6%; the percentage of shaly limestone thickness is 25.8%; the percentage of limy shale thickness is 7.7% (Figure 10B). These quantitative parameters reveal the characteristics of the different lithologies. As reservoir rocks, the individual thicknesses of the shaly limestone and argillaceous limestone are medium, and the number of layers is large. The total thicknesses of these two lithologies are the greatest. As cap and interlayer rocks, the individual layer thicknesses of salt and anhydrite are large, but the number of layers is small. The total thickness of these two lithologies is the second. As source rocks, the single-layer thickness of limy shale is the smallest, generally not exceeding 1 m, and the total thickness is the smallest.

5.2 Lithological characteristics in horizontal formation

During the deposition of the Middle Triassic Leikoupo Formation, uplifts were developed at the edge of the basin. The saline seawater was evaporated in the restricted platform in the arid paleoclimate. From the center to the margin of the Sichuan Basin, the depositional facies are anhydrite-salt lagoon, marly lagoon, lagoon margin of marly flat, dolomitic flat, and marly flat (Figure 1B).

Based on the lithological identification results in individual boreholes, the lithological characteristics in the horizontal formation are interpreted in different depositional facies (Figure 11). The salt, as regional cap rock, is the thickest in the central anhydrite-salt lagoon and thins towards the basin margin. The total thickness percentage of salt is reduced from the central to the marginal in the basin. The number of layers and the total thickness of anhydrite decrease towards the margin of the basin as well. Thin interbedded argillaceous limestone, shaly limestone, and limy shale are separated by anhydrite. The number of marl layers in the central basin is greater than in the marginal basin; The monolayer thickness and total percentage of marl thickness in the central basin are less than in the marginal basin. Gases are well trapped in these thin marls.

5.3 Lithological characteristics of the region

Based on lithological identification results in 119 wells, thickness contour plans of each lithology are generated in the survey region. The first-order lithologies are shown in Figure 12. Anhydrite is developed in the center with NE-SW, and the maximum thickness is in the northeast. The anhydrite cap rock is region-wide (Figure 12A). Salt is just dominated in the southeast, with no development in the northwestern (Figure 12B). The distribution of the marl is relatively wide and developed throughout the area, mainly concentrated in the center NE-SW region (Figure 12C). The different marl lithologies are shown in Figure 13. Regional features of the preponderant reservoir, interlayer, and source rock are clear. As an unconventional reservoir, the thickness of anhydrite marl, argillaceous limestone, shaly limestone, and limy shale are crucial factors for further geological understanding. These lithological characteristics of the region would offer an important reference for subsequent exploration and development of natural gas.

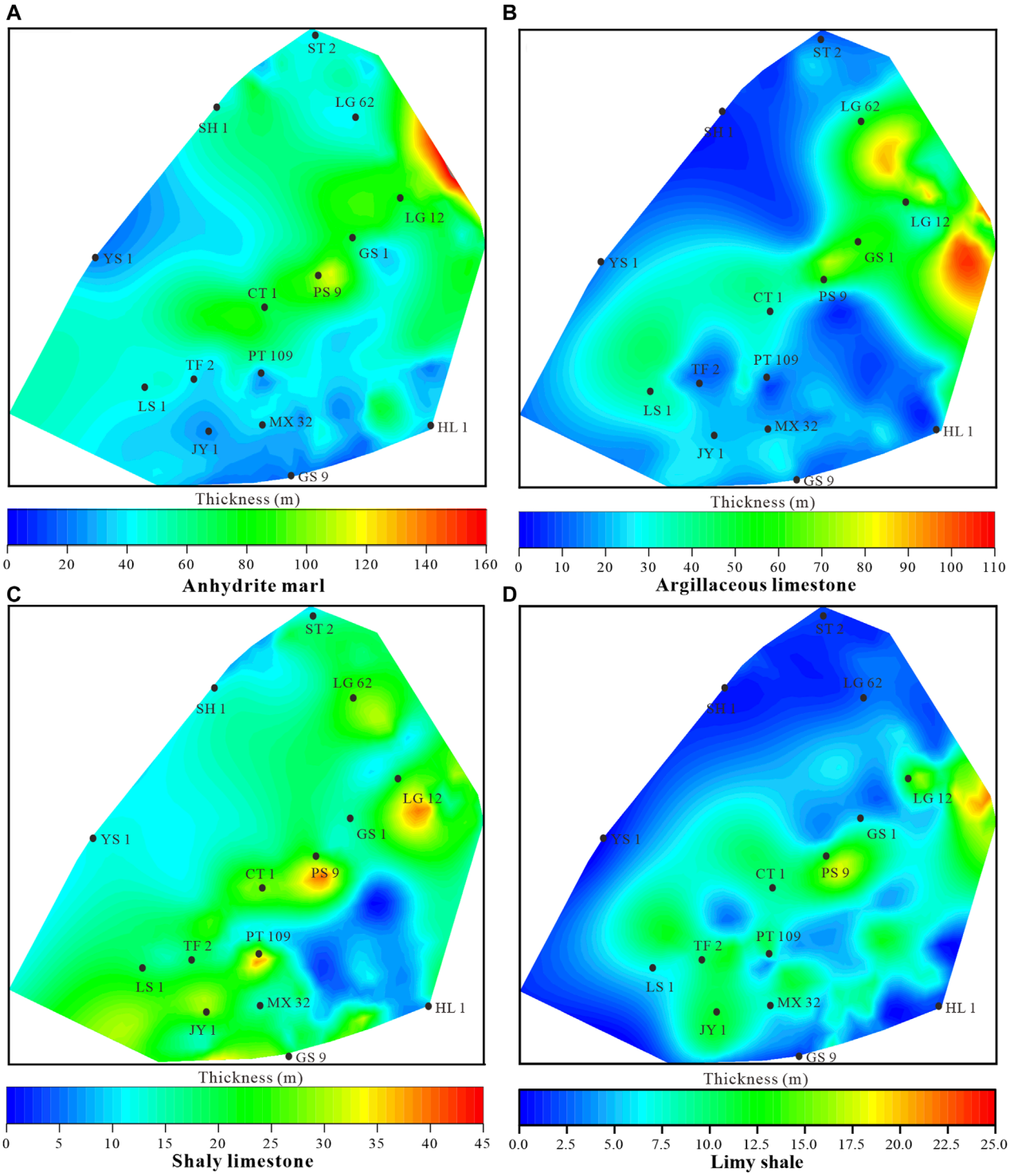

FIGURE 13
Lithological thickness plane spread of marl in $T_2l_3^2$. **(A)** Thickness plane spread of anhydrite marl. **(B)** Thickness plane spread of argillaceous limestone. **(C)** Thickness plane spread of shaly limestone. **(D)** Thickness plane spread of limy shale.

6 Conclusion

(1) Lithological identification of 2D and 3D plots is established for the complex marl reservoir in $T_2l_3^2$ of the Sichuan Basin. Identification standard of the first-order lithology is: salt GR<35 API, DEN<2.5 g/cm^3, RT>3,000 Ω·m; anhydrite GR<35 API, DEN>2.7 g/cm^3, RT>800 Ω·m; marl GR>30 API, RT<2000 Ω·m, DEN 2.5–2.8 g/cm^3. Identification standard of the fine lithology in marl is: anhydrite marl GR<35 API, RT 800–2000 Ω·m; argillaceous limestone GR

30–50 API, RT 200–2000 Ω·m; shaly limestone GR 40–60 API, RT 30–300 Ω·m; limy shale GR>45 API, RT<80 Ω·m.

(2) In the coring interval, the coincidence rate of identifying lithological results is larger than 90%. As reservoir rocks, the individual thicknesses of the shaly limestone and argillaceous limestone are medium, and the number of layers is large. As cap and interlayer rocks, the individual layer thicknesses of salt and anhydrite are large, but the number of layers is small. As source rock, the single-layer thickness of limy shale is the smallest, generally not exceeding 1 m.

(3) The anhydrite cap rock is region-wide, while salt is just dominated in the southeastern, with no development in the northwestern. The distribution of the marl is relatively wide and developed throughout the area, mainly concentrated in the center NE-SW region. The plane thickness of anhydrite marl, argillaceous limestone, shaly limestone, and limy shale have practical significance for follow-up exploration in $T_2l_3^2$ of the central Sichuan Basin.

Data availability statement

The data analyzed in this study is subject to the following licenses/restrictions: The dataset not available. Requests to access these datasets should be directed to ZW, 2022710367@yangtzeu.edu.cn.

Author contributions

RY: Writing–original draft, Writing–review and editing. ZW: Conceptualization, Data curation, Formal Analysis, Methodology, Software, Visualization, Writing–original draft. YX: Resources, Visualization, Writing–review and editing. HZ: Data curation, Formal Analysis, Writing–review and editing. SW: Methodology, Writing–review and editing. SY: Formal Analysis, Writing–original draft.

Funding

The author(s) declare that no financial support was received for the research, authorship, and/or publication of this article.

Acknowledgments

The reviewers are gratefully acknowledged for constructive comments that substantially improved the quality of this manuscript. Also, we appreciate the editor's suggestions to revise this manuscript.

Conflict of interest

The authors declare that the research was conducted in the absence of any commercial or financial relationships that could be construed as a potential conflict of interest.

Publisher's note

References

Afsar, F., Westphal, H., and Philipp, S. L. (2014). How facies and diagenesis affect fracturing of limestone beds and reservoir permeability in limestone–marl alternations. *Mar. Pet. Geol.* 57, 418–432. doi:10.1016/j.marpetgeo.2014.05.024

Balumi, W. B., Elghonimy, R. S., Sonnenberg, S., and Puckette, J. (2022). Chemostratigraphy of unconventional shale reservoirs: a case study of the Niobrara Formation within the Denver-Julesburg Basin. *Mar. Pet. Geol.* 146, 105957. doi:10.1016/j.marpetgeo.2022.105957

Ben, C. N., Khemiri, F., Soussi, M., Latil, J. L., Robert, E., and Belhajtaher, I. (2019). Aptian-Lower Albian Serdj carbonate platform of the Tunisian Atlas: development, demise and petroleum implication. *Mar. Pet. Geol.* 101, 566–591. doi:10.1016/j.marpetgeo.2018.10.036

Brekke, H., MacEachern, J. A., Roenitz, T., and Dashtgard, S. E. (2017). The use of microresistivity image logs for facies interpretations: an example in point-bar deposits of the McMurray Formation, Alberta, Canada. *AAPG Bull.* 101 (5), 655–682. doi:10.1306/08241616014

Carrasquilla, A., and Caetano, L. (2021). Proportional integral derivative controller used to simulate the mineral concentration and fluid saturations from geological data and well logs in the Namorado reservoir, Southeastern Brazil. *J. South Am. Earth Sci.* 111 (Nov), 103455–103455.10. doi:10.1016/j.jsames.2021.103455

Chen, J. X., Guo, Z. L., He, Z. L., Tao, Z., Zhu, H. H., Luo, T., et al. (2022). Maturity assessment of solid bitumen in the Sinian carbonate reservoirs of the eastern and central Sichuan Basin, China: Application for hydrocarbon generation modelling. *Geol. J.* 57 (11), 4662–4681. doi:10.1002/gj.4564

Cherif, A., Naimi, M. N., and Belaid, M. (2021). Deep-sea trace fossils and depositional model from the lower Miocene Tiaret marl formation (northwestern Algeria). *J. Afr. Earth Sci.* 175 (Mar), 104115–104115.16. doi:10.1016/j.jafrearsci.2021.104115

Folkestad, A., Veselovsky, Z., and Roberts, P. (2012). Utilising borehole image logs to interpret delta to estuarine system: a case study of the subsurface Lower Jurassic Cook Formation in the Norwegian northern North Sea. *Mar. Pet. Geol.* 29 (1), 255–275. doi:10.1016/j.marpetgeo.2011.07.008

Kumar, M., Dasgupta, R., Singha, D. K., and Singh, N. P. (2018). Petrophysical evaluation of well log data and rock physics modeling for characterization of Eocene reservoir in Chandmari oil field of Assam-Arakan Basin India. *J. Pet. Explor Prod. Technol.* 8 (2), 323–340. doi:10.1007/s13202-017-0373-8

Liao, Z. H., Wu, M. N., Chen, X. F., and Zou, H. Y. (2020). Fracture mechanical properties of carbonate and evaporite caprocks in Sichuan Basin, China with implications for reservoir seal integrity. *Mar. Pet. Geol.* 119, 104468–104471. doi:10.1016/j.marpetgeo.2020.104468

Lü, Y. Z., Ni, C., Zhang, J. Y., Gu, M. F., Sun, Q. F., Liu, Z. S., et al. (2013). Favorable sedimentary facies zones and lithofacies palaeogeography of middle Triassic Leikoupo Formation in Sichuan Basin. *Mar. Ori Pet. Geol.* 18 (1), 26–32. doi:10.3969/j.issn.1672-9854.2013.01.004

Luo, X. P., Pang, X., Su, D. X., Lu, H., Zhang, N., and Wang, G. (2018). Recognition of complicated sandy conglomerate reservoir based on micro-resistivity imaging logging: a case study of Baikouquan Formation in western slope of Mahu Sag, Junggar Basin. *Xinjiang Petrol Geol.* 39 (3), 345–351. doi:10.7657/XJPG20180313

Ma, Y. S., Zhang, Y. C., Guo, T. L., Zhu, G., Cai, X., and Li, M. (2008). Petroleum geology of the Puguang sour gas field in the Sichuan Basin, SW China. *Mar. Pet. Geol.* 25 (4/5), 357–370. doi:10.1016/j.marpetgeo.2008.01.010

Meng, Q. Q., Li, J. Z., Liu, W. H., Fu, Q., Wang, X. F., and Wang, J. (2022). Simulation study on the effect of anhydrite-salt content on hydrocarbon generation in mature stage shale. *Spe Oil Gas Reserv* 29 (5), 113–118. doi:10.3969/j.issn.1006-6535.2022.05.016

Paul, H. N., and Stephen, N. E. (2006). Sandstone vs carbonate petroleum reservoirs: a global perspective on porosity-depth and porosity-permeability relationships: Reply. *AAPG Bull.* 90 (5), 811–813. doi:10.1306/11070505163

Ramos, L. D. M., and Neves, A. A. J. (2019). Lithology identification on well logs by fuzzy inference. *J. Pet. Sci. Eng.* 180, 357–368. doi:10.1016/j.petrol.2019.05.044

Saporetti, C. M., Da Fonseca, L. G., and Pereira, E. (2019). A lithology identification approach based on machine learning with evolutionary parameter tuning. *IEEE Geosci. Remote Sens. Lett.* 16 (12), 1819–1823. doi:10.1109/LGRS.2019.2911473

Shen, A. J., Zhou, J. G., Xin, Y. G., and Luo, X. Y. (2008). Origin of Triassic Leikoupo dolostone reservoirs in Sichuan Basin. *Mar. Ori Petro Geol.* 13 (4), 19–28. doi:10.3969/j.issn.1672-9854.2008.04.004

Shen, J. J., Chen, B., Wang, C. L., Chang, J. J., Zhou, X. F., Guan, X. Q., et al. (2015). Sedimentary characteristics and control factors of anhydrite-salt rocks in the Paleogene Xingouzui formation in Jiangling Depression, Jianghan basin. *J. Palaeogeogr. (China Ed.* 17 (2), 265–274. doi:10.7605/gdlxb.2015.02.022

Tan, L., Liu, H., Tang, Q. S., Li, F., Tang, Y. Z., Liang, F., et al. (2021). Application of seismic geomorphology to carbonate rocks: a case study of the Cambrian Longwangmiao formation in the Gaoshiti-Moxi area, Sichuan Basin, China. *Mar. Pet. Geol.* 126, 104919–104921. doi:10.1016/j.marpetgeo.2021.104919

Tan, X. C., Li, L., Liu, H., Luo, B., Zhou, Y., Wu, J., et al. (2011). General depositional features of the carbonate platform gas reservoir of the Lower Triassic Jialingjiang Formation in the Sichuan Basin of southwest China: Moxi gas field of the central basin. *Carbonates Evaporites* 26 (4), 339–350. doi:10.1007/s13146-011-0070-5

Tian, H., Feng, Q. F., Xin, Y. G., and Zhang, H. (2020). Well logging petrophysical experiment analysis of dolomite reservoir in Leikoupo Formation in Zhongba Area. *Well Logging Techno* 44 (5), 438–442. doi:10.16489/j.issn.1004-1338.2020.05.003

Tian, H., Tang, S., Zhang, J. Y., Xin, Y. G., Wang, X., and Li, Z. W. (2018). Characteristics and formation conditions of carbonate reservoir in Leikoupo Formation of western Sichuan Basin. *Nat. Gas. Geosci.* 29 (11), 1585–1594. doi:10.11764/ji.ssn.1672-1926.2018.08.010

Tian, H., Wang, G. W., Duan, S. F., Xin, Y. G., and Zhang, H. (2021). Reservoir characteristics and exploration target of the middle Triassic Leikoupo Formation in Sichuan Basin. *China Pet. Explor* 26 (5), 60–73. doi:10.3969/j.issn.1672-7703.2021.05.006

Wang, L., He, Y. M., Peng, X., Deng, H., Liu, Y. C., and Xu, W. (2020). Pore structure characteristics of an ultradeep carbonate gas reservoir and their effects on gas storage and percolation capacities in the Deng IV member, Gaoshiti-Moxi Area, Sichuan Basin, SW China. *Mar. Pet. Geol.* 111, 44–65. doi:10.1016/j.marpetgeo.2019.08.012

Wang, X., Xin, Y. G., Tian, H., Zhu, M., Zhang, H., and Li, W. Z. (2020). Research progress on sedimentation and reservoir of Leikoupo Formation of middle Triassic in Sichuan Basin. *Mar. Ori Pet. Geol.* 25 (3), 210–222. doi:10.3969/j.issn.1672-9854.2020.03.003

Wang, Y. X., Zhou, W., Guo, R., Fu, M. Y., Shen, Z. M., Zhao, L. M., et al. (2016). Characteristics and origin of high porosity and low permeability carbonate reservoirs in the Sa'di Formation, Halfaya Oil Field, Iraq. *Pet Geol Exp.* 38 (2), 224–230. doi:10.11781/sysydz201602224

Wang, Z. C., Xin, Y. G., Xie, W. R., Wen, L., Zhang, H., Xie, Z. Y., et al. (2023). Petroleum geology of marl in Triassic Leikoupo Formation in central Sichuan Basin and discovery significance of Chongtan1 well. *Pet. Explor Dev.* 50 (5), 950–961. doi:10.11698/PED.20220715

Xin, Y. G., Wen, L., Zhang, H., Tian, H., Wang, X., Sun, H. F., et al. (2022). Study on reservoir characteristics and exploration field of the middle Triassic Leikoupo Formation in Sichuan Basin. *China Pet. Explor* 27 (4), 91–102. doi:10.3969/j.issn.1672-7703.2022.04.007

Xin, Y. G., Zheng, X. P., Zhou, J. G., Ni, C., Gu, M. F., Gong, Q. S., et al. (2013a). Characteristics and distribution of reservoirs in the Lei-3^3 of the Leikoupo Formation in the western central Sichuan Basin. *Nat. Gas. Ind.* 33 (3), 5–9. doi:10.3787/j.issn.1000-0976.2013.03.002

Xin, Y. G., Zhou, J. G., Ni, C., Gu, M. F., Gong, Q. S., Dong, Y., et al. (2013b). Sedimentary facies features and favorable lithofacies distribution of Middle Triassic Leikoupo barriered carbonate platform in Sichuan Basin. *Mar. Ori Pet. Geol.* 18 (2), 1–7. doi:10.3969/j.issn.1672-9854.2013.02.001

Xu, C. M., Cronin, T. P., McGinness, T. E., and Steer, B. (2009). Middle Atokan sediment gravity flows in the Red Oak field, Arkoma Basin, Oklahoma: a sedimentary analysis using electrical borehole images and wireline logs. *AAPG Bull.* 93 (1), 1–29. doi:10.1306/09030808054

Xu, Z. P., Chen, S. P., Luo, C. M., Yang, G., Xu, S. D., Hu, F. J., et al. (2023). Distribution and sealing capacity evaluation of anhydrite-salt rocks in the Middle Cambrian in Tarim Basin. *China Pet. Explor* 28 (5), 54–67. doi:10.3969/j.issn.1672-7703.2023.05.005

Yan, J. P., Cai, J. G., Zhao, H. M., Li, Z. Z., and Xu, G. H. (2011). Application of electrical image logging in the study of sedimentary characteristics in sandy conglomerates. *Petrol Explor Devel.* 38 (4), 445–451.

Yang, Y., Xie, J. R., Zhang, J. Y., Wen, L., Zhao, L. Z., Zhang, H., et al. (2022). Characteristics and exploration potential of unconventional middle Triassic Lei3^2 reservoirs in the central Sichuan Basin. *Nat. Gas. Ind.* 42 (12), 12–22. doi:10.3787/j.issn.1000-0976.2022.12.002

Yin, S. J., Wen, Z., Jin, X. Y., Yan, W. L., Wang, C. Y., Shi, J. B., et al. (2023). Characteristics and logging characterization method of unconventional marl reservoir: a case study of the Member 1 of Maokou Formation in Hechuan-Tongnan Area, Sichuan Basin. *Acta Pet. Sin.* 44 (7), 1105–1117. doi:10.7623/syxb202307007

Yuan, R., Yang, B., Pan, C. F., Guo, X. G., Huang, L. L., He, W. J., et al. (2020). Conglomerate petrology characterization using high-definition borehole electrical images in the Upper Urho Formation at well JL42, Zhongguai Uplift, Junggar Basin, China. *Interpretation* 8 (3), SL137–SL150. doi:10.1190/INT-2019-0243.1

Zhang, H., Xin, Y. G., and Tian, H. (2021). Gas-bearing property prediction of Leikoupo Formation in the northwest Sichuan Basin based on the theory of two-phase media. *Geophy Geoche Explor* 45 (6), 1386–1393. doi:10.11720/wtyht.2021.1340

Zhang, J., Nie, X., Xiao, S. Y., Zhang, C., and Zhang, Z. (2018). Generating porosity spectrum of carbonate reservoirs using ultrasonic imaging log. *Acta geophys.* 66 (2), 191–201. doi:10.1007/s11600-018-0134-1

Zhang, J. Y., Xin, Y. G., Zhang, H., Tian, H., Zhu, X. J., and Chen, W. (2023). A new unconventional gas reservoir type: source-reservoir integrated carbonate gas reservoir from evaporated lagoon facies in Lei_3^2 sub-member in Central Sichuan Basin. *Nat. Gas. Geosci.* 34 (1), 23–34. doi:10.11764/j.issn.1672-1926.2022.10.012

Zhang, Q. Y., Shi, W. X., Liu, X., Hui, G. J., and Yuan, C. Y. (2022). Application of hyperspectral scanning in mineral composition analysis of carbonate rocks. *Rock Min. Anal.* 41 (5), 815–825. doi:10.15898/j.cnki.11-2131/td.202112100200

Zhou, J. G., Xin, Y. G., Gu, M. F., Zhang, J. Y., Hao, Y., Li, G. J., et al. (2010). Direction of gas exploration in the middle Triassic Leikoupo Formation of the Sichuan Basin. *Nat. Gas. Ind.* 30 (12), 16–19+121. doi:10.3787/j.issn.1000-0976.2010.12.004

Zhou, L. X. (2008). Application of Fullbore formation Microimager (FMI) to study of glutenite sedimentary structures in Jiyang Depression. *Xinjiang Petrol Geol.* 29 (5), 654–656.